Fractional Delay and Fractional Doppler Estimation and Mitigation Framework in OTFS Systems

Salah Eddine Zegrar, *Member, IEEE*, Ahmet Sacid Sümer, and Hüseyin Arslan, *Fellow, IEEE*

***Abstract*—Orthogonal time-frequency space (OTFS) modulation is fast becoming a popular modulation scheme for high-mobility wireless communication due to its ability to render time-varying channels invariant and sparse. However, due to the limited time duration and frequency bandwidth of the transmitted OTFS signal, the occurrence of fractional delay and Doppler shifts becomes inevitable, causing both inter-delay interference (IDeI) and inter-Doppler interference (IDI). In this paper, an impulse-based channel estimation method is used, which takes advantage of the fact that the pilot impulse is a pulse tone (pulsone). A pulsone maintains its shape despite time delay and Doppler shift operations, as well as being self-dual between time and frequency domains. Exploiting these two features, a low-complexity algorithm is proposed to estimate the fractional delay and fractional Doppler channel. We derive the Cramer-Rao lower bound (CRLB) of the estimated fractional channel and show that the developed estimator is efficient. Then, we provide the computational complexity analysis of the proposed algorithm. After that, we show and stress that the proposed channel estimation scheme is better in terms of the channel normalized mean squared error (NMSE) and the bit-error rate (BER). Lastly, the simulation results are confirmed via real experimental results.**

***Index Terms*—OTFS, channel estimation, pulsone, fractional delay, fractional Doppler, inter-delay interference, inter-Doppler interference (IDI).**

I. Introduction

Fifth generation (5G) communication systems signaled a paradigm shift in wireless networks by introducing concepts services such as ultra-reliable low latency communications (URLLC) and massive machine type communications (mMTC), in addition to the improvement of data rates for enhanced mobile broadband (eMBB). These new services focused on improving the connectivity and reliability of communication to enable new use cases such a autonomous driving, remote healthcare, industrial automation, and so on. The diversity of applications is expected to expand even further in 6G systems resulting in services such as services like further-enhanced mobile broadband (FeMBB), extremely-RLLC (ERLLC), ultra-mMTC (umMTC), extremely low-power communication (ELPC), long-distance and high-mobility communication (LDHMC) [1], [2]. While the former services can be considered as extensions of the earlier ones seen in 5G, the last one presents several new challenges [3]. High mobility leads to increasingly selective channel and Doppler spread. Given that 5G uses OFDM at its physical layer, Doppler spread leads to severe performance degradation due to inter-carrier interference (ICI) between the subcarriers. As such, it is important to design a waveform that is able to mitigate mobility issues [4], [5].

Recently, orthogonal time-frequency space (OTFS) modulation has been proposed as a robust waveform suitable for doubly-dispersive channels as in high mobility scenarios [6]. For any waveform, OTFS modulation parameterizes the effect of the time-varying channels by representing the channel in the delay-Doppler domain, where the reflectors distributed in the propagation environment correspond to the channel seen at the receiver, and thus, for a relatively short time frame the channel can be considered invariant [7].

One of the most critical challenges pertaining to the OTFS waveform is channel estimation, which is necessary to equalize the signal and demodulate the data. For instance, impulse-based channel estimation is used in [8], [9] to estimate the OTFS multiple-input multiple-output (MIMO) channel. In particular, in [8] delay-Doppler impulses are adopted as pilots for channel estimation, while message passing algorithm is used for symbol detection. OTFS exhibits delay-Doppler-angle 3D sparsity in massive MIMO (mMIMO) systems, and accordingly, 3D structured orthogonal matching pursuit (3D-SOMP) based channel estimation technique is used with low pilot overhead. The authors in [9] used the expectation maximization-based variational Bayesian (EM-VB) method in order to obtain Doppler shift, delays, angles, and channel gains in the uplink channel. Then, reciprocity is exploited to estimate the downlink channel parameters at the base station. In order to increase the spectral efficiency, [10] used superimposed pilots with a data-aided channel estimation algorithm, where the guard band is not used anymore and the pilot-data interference is mitigated with iterative data detection. Moreover, compressed sensing-based delay-Doppler channel estimation is proposed for OTFS multiple access systems in [11]. In [12], a 2D structured turbo compressed sensing-based channel estimation method is proposed

Received 24 March 2024; revised 2 July 2024; accepted 21 September 2024. Date of publication 30 September 2024; date of current version 14 February 2025. This work was supported by the Scientific and Technological Research Council of Türkiye (TUBITAK) under Grant 123E514. The review of this article was coordinated by Prof. Yiqing Zhou. *(Corresponding author: Salah Eddine Zegrar.)*

Salah Eddine Zegrar is with the Department of Electrical and Electronics Engineering, Istanbul Medipol University, Istanbul 34810, Türkiye, and also with the ULAK Haberleşme, Istanbul 34906, Türkiye (e-mail: zegrarsalaheddine@gmail.com, salah.zegrar@medipol.edu.tr).

Ahmet Sacid Sümer and Hüseyin Arslan are with the Department of Electrical and Electronics Engineering, Istanbul Medipol University, Istanbul 34810, Türkiye (e-mail: ahmet.sumer1@medipol.edu.tr; huseyinarslan@medipol.edu.tr).

Digital Object Identifier 10.1109/TVT.2024.3470839

for the high mobility scenarios. Additionally, a sparse Bayesian learning-based channel estimation method is studied in [13] with a new pilot pattern without a guard. This new pattern converts the channel estimation problem into a sparse signal recovery problem.

These studies [8], [9], [10], [11], [12], [13], however, only consider integer delay-Doppler scenarios, which are impractical in real-world implementations where fractional delay and Doppler shifts are always present. Therefore, the authors in [14] proposed a low-complexity message-passing algorithm which mitigates the highest inter-Doppler interference (IDI) components for OTFS channel estimation. This work was followed by [15], where delay-Doppler embedded pilot symbols are adopted for channel estimation using the threshold method. Furthermore, in [16], Raviteja et al. arranged the pilot, guard, and data such that interference is avoided. Delay-Doppler domain embedded pilot-based time domain channel estimation method is proposed in [17] considering carrier frequency offset, residual frame timing offset, and fractional Doppler shifts, which are further used to construct channel estimation and equalization methods. Shi et al. investigated MIMO OTFS systems and proposed a modified sensing matrix-based channel estimation with a deterministic pilot design for a downlink channel state information (CSI) acquiring scheme [18]. In [19], the OTFS channel is estimated using pilots in the delay-Doppler domain with a cross-correlation-based algorithm. This method has lower computational complexity than the traditional channel estimation methods with pseudo sequences. In [20], two superimposed pilot-aided channel estimation methods are proposed. The first method considers data as interference and estimates the channel. However, it degrades the signal-to-noise ratio (SNR). The second method reduces the degradation of SNR by exploiting the iterations between data detection and channel estimation. The authors in [21] adopted Bayesian learning, which formulates the problem as sparse signal recovery. Then, the channel gains along with the fractional Doppler shifts are estimated rather than estimating the delay-Doppler domain channel directly. The authors in [22] adopted sparse Bayesian learning for off-grid actual delay-Doppler domain channel response estimation rather than effective channel response, which is investigated in the literature. The OTFS channel estimation is formulated as sparse signal recovery where both delays and Doppler shifts are estimated separately; however, this suffers from high computational complexity, especially in the case of having doubly-spreading channels.

However, in these works [15], [16], [17], [18], [19], [20], [21], only fractional Doppler shifts were of concern, even though fractional delays occur with the same likelihood in OTFS systems as fractional Doppler shifts. Moreover, considering only wideband signals for OTFS system to provide sufficient delay resolution limits the potential of this waveform. OTFS should be flexible enough to freely tune the bandwidth $(M\Delta f)$ and the time duration (NT) of the signal based on the application and user requirement instead of delay and Doppler resolution. Moreover, [22] suffer from high computational complexity which also limit the use of this method.

In this paper, we propose a framework that can be adopted to estimate fractional Doppler and fractional delay channels using impulse-based channel estimation. The pilot, being an impulse, can be seen as a single OTFS subcarrier or pulsone (pulse-tone), which has two main properties: 1) it holds its shape under the operations of time delay and Doppler shift, as well as 2) being self-dual between time and frequency. Exploiting these two features, a low-complexity algorithm is proposed where we raise the received pilot pulsone to higher powers in both time and frequency domains to estimate fractional Doppler and delay shifts, respectively. By raising the received time-pulsone/frequency-pulsone to the α-power, which serves as a scaling factor that controls the extent of delay or Doppler shift applied to an OTFS carrier, we can tune the Doppler shifts or delay shifts until we find an option ($\alpha = \alpha_{\text{opt}}$) that converts both fractional delay and Doppler shifts to integer ones. These fractional shifts are then calculated using α_{opt}.

The contributions of this paper are summarized as follows:

- We propose a general channel estimation and equalization framework that can be applied to estimate and equalize both fractional delays and Doppler shifts. A complete wireless communication OTFS system model is considered, assuming the multi-tap channel to be doubly-dispersive in both time and frequency domains, including residual delays and Doppler shifts. This framework is based on the fact that an impulse-pilot is shape-invariant under the operations of time delay and Doppler shift, as well as being self-dual between time and frequency.
- The proposed method achieves fine-resolution estimation of the fractional delay and Doppler shifts by attaining the lowest possible mean squared error among all unbiased methods. The proposed estimator's performance converges to the Cramer-Rao lower bound (CRLB) performance; thus, it is *efficient estimator*. On top of that, We show that the proposed framework provides the flexibility to adapt the computational complexity according to the required delay and Doppler resolution. This makes it implementable in low-cost, limited-power devices such as internet-of-things (IoT) devices.
- We derive the tensor form of the input-output relationship between the transmitted and received signals in the case of fractional delay channels by introducing the upsampled channel matrix. Then, the minimum mean squared error (MMSE) detector is derived to equalize the effect of the fractional delay channel.
- Finally, the proposed method's practicality and efficiency are confirmed by testing and evaluating it in a real-time experiment using the Keysight Agilent Technologies EXA signal analyzer N9010A.

The rest of this paper is organized as follows; Section II introduces the system model used for OTFS transmission and reception. In Section III, we define and formulate the problem. In Section IV, we introduce and proof the properties of the pulsone. The proposed fractional delay and Doppler channel estimation and equalization framework is discussed in Section V. The performance metrics are derived in Section VI. In Section VII,

the simulation results are analysed and discussed. Finally, Section VIII concludes the paper.[1]

II. System Model

In this section, the OTFS system model, comprising transmitter, channel, and receiver, is introduced. Then, the input-output relationship of the received signal is investigated for various doubly-dispersive channel scenarios.

A. Transmitter

Consider $M \times N$ information symbols $\{X(l,k), l = 0,\ldots,M-1;\ k = 0,\ldots,N-1\}$ distributed over the two-dimensional (2D) delay-Doppler grid. These symbols are modulated and mapped onto 2D time-frequency domain $\{\mathcal{X}[m,n],\ m = 0,\ldots,M-1;\ n = 0,\ldots,N-1\}$ using OTFS modulation. M and N refer to total delay and Doppler bins, respectively. The delay-Doppler symbols are converted to the time-frequency grid $X[n,m]$ via the inverse symplectic finite Fourier transform (ISFFT) as follows

$$\mathcal{X}[m,n] = \frac{1}{\sqrt{MN}} \sum_{l=0}^{M-1} \sum_{k=0}^{N-1} X(l,k) e^{j2\pi\left(\frac{nk}{N} - \frac{ml}{M}\right)}. \quad (1)$$

The time-frequency grid sampling intervals can be defined by T symbol duration and $\Delta f = 1/T$ subcarrier spacing. Therefore, total symbol duration and bandwidth are represented as NT and $M\Delta f$, respectively. This implies a spacing of $\frac{1}{M\Delta f}$ and $\frac{1}{NT}$ between adjacent delay and Doppler bins, respectively.

Using Heisenberg transform, $\mathcal{X}[m,n]$ can be transformed to one-dimensional time domain signal $s(t)$ as follows

$$s(t) = \sum_{n=0}^{N-1} \sum_{m=0}^{M-1} \mathcal{X}[m,n] e^{j2\pi m\Delta f(t-nT)} g_{\text{tx}}(t-nT), \quad (2)$$

where g_{tx} is the transmitted pulse shape. Considering that rectangular pulse shapes are used at both transmitter and receiver, the transmitted signal can be expressed as

$$s(t) = \sum_{n=0}^{N-1} \sum_{m=0}^{M-1} \text{rect}\left(\frac{t-nT}{T}\right) \mathcal{X}[m,n] e^{j2\pi m\Delta f(t-nT)} \quad (3)$$

where rect (t) is the rectangular pulse function. Finally, in order to combat the channel effect and provide circularity, we append a cyclic prefix (CP) of length M_{cp} as given in [23]. To cast (1) from serial to matrix-vector form, we define $\mathbf{F}_N$ to be the $N \times N$ unitary discrete Fourier transform (DFT) matrix; therefore, (1) is rewritten as

$$\mathbf{X}_{\text{TF}} = \mathbf{F}_M \mathbf{X}_{\text{DD}} \mathbf{F}_N^H. \quad (4)$$

Next, $\mathbf{X}_{\text{TF}}$ is converted to time signal $\mathbf{s}$ by applying the Heisenberg transform. Then, $\mathbf{s}$ is transmitted over the doubly-dispersive channel as follows

$$\mathbf{s} = \text{vec}\,(\mathbf{S}) = (\mathbf{F}_N^H \otimes \mathbf{I}_M)\mathbf{x}, \quad (5)$$

where $\mathbf{S} = \mathbf{X}_{\text{DD}}\mathbf{F}_N^H$, $\mathbf{x} = \text{vec}(\mathbf{X}_{\text{DD}})$, and $\mathbf{I}_M$ denotes the $M \times M$ identity matrix.

B. Wireless Channel

Consider the doubly-dispersive channel with L-taps modeling L reflectors in the propagation environment as follows

$$h(\tau,\nu) = \sum_{i=0}^{L-1} h_i \delta(\tau - \tau_i)\delta(\nu - \nu_i), \quad (6)$$

where h_i and L denote the complex channel gain and number of propagation paths, respectively. The delay and Doppler shifts corresponding the i-th reflector with l_i and k_i integer delay and Doppler indices are respectively given by $\tau_i = \frac{l_i+\iota_i}{M\Delta f}$ and $\nu_i = \frac{k_i+\kappa_i}{NT}$ where ι_i and $\kappa_i \in [-0.5, 0.5]$ represent the fractional delay and Doppler indices of the i-th path of the channel. For channel estimation, in this paper, the impulse-based channel estimation is adopted [16], where one pilot X_p having $\text{SNR}_p = |X_p|^2/\sigma^2$ is placed in the delay-Doppler grid surrounded by guard symbols (σ^2 denotes the noise variance). The guard is inserted to insure that no interference occurs between the data symbols and the pilot after passing through the channel. Therefore, the guard and pilot arrangement differs depending on the channel scenarios.

C. Receiver

The transmit signal passes through the L-tap doubly-dispersive fading channel given in (6). Then, the received signal $r(t)$ can be represented as

$$r(t) = \sum_{i=0}^{L-1} h_i e^{j2\pi\nu_i(t-\tau_i)} s(t-\tau_i). \quad (7)$$

At the receiver side, matched filtering applied with receiver pulse shape $g_{\text{rx}}(t)$. This filtering operation is defined by cross-ambiguity function $A_{g_{\text{rx}},r}(\tau,\nu)$ and can be expressed as

$$A_{g_{\text{rx}},r}(\tau,\nu) \triangleq \int e^{-j2\pi\nu(t-\tau)} g_{\text{rx}}^*(t-\tau) r(t) dt. \quad (8)$$

Sampling the cross-ambiguity function at the given points, the time-frequency domain symbols $\mathcal{Y}[n,m]$ obtained as

$$\mathcal{Y}[n,m] = A_{g_{\text{rx}},r}(\tau,\nu)|_{\tau=nT,\nu=m\Delta f}. \quad (9)$$

This transformation is also known as the Wigner transform, which is the inverse of the Heisenberg transform.

The received time-frequency signal $\mathcal{Y}(n,m)$ is converted back to delay-Doppler domain via symplectic finite Fourier

[1] *Notation:* Bold uppercase $\mathbf{A}$, bold lowercase $\mathbf{a}$, and unbold letters A, a denote matrices, column vectors, and scalar values, respectively. $(\cdot)^H$, $(\cdot)^T$, and $(\cdot)^{-1}$ denote the Hermitian, transpose, and inverse operators. $[\alpha]_\beta$ takes modulo-β of α. $\delta(\cdot)$ and $\angle$ denote the Dirac-delta function and phase representation. $\text{E}(\cdot)$ and $\mathcal{F}\{\cdot\}$ denote the expectation and Fourier transform operator. $\text{diag}(A_1,\ldots,A_N)$ and $\text{BlkDiag}(\mathbf{A}_1,\ldots,\mathbf{A}_N)$ returns the diagonal and block diagonal matrices composed of $A_1,\ldots,A_N$ and $\mathbf{A}_1,\ldots,\mathbf{A}_N$ in their diagonal, respectively. $\mathbb{C}^{M\times N}$ denotes the space of $M \times N$ complex-valued matrices, and $\text{vec}(\cdot)$ denotes the vectorization operator. $\mathbf{A} \otimes \mathbf{B}$ is the Kronecker product of $\mathbf{A}$ and $\mathbf{B}$ and symbol j represents the imaginary unit of complex numbers with $j^2 = -1$.

transform (SFFT) as follows

$$Y(l,k)=\sum_{n=0}^{N-1}\sum_{m=0}^{M-1}\mathcal{Y}(n,m)e^{-j2\pi\left(\frac{nk}{N}-\frac{ml}{M}\right)}. \tag{10}$$

III. Problem Formulation

Most of the recent studies assume only fractional Doppler shifts in OTFS systems, where they assume wideband OTFS transmitted signals in order to provide enough delay resolution, thus integer delay shifts. However, this assumption limits the potential of this waveform and forces OTFS signals to have a fixed time-frequency distribution which is undesired in the next wireless generations. OTFS should be flexible enough to freely tune the bandwidth ($M\Delta f$) and the time duration ($NT=\frac{N}{\Delta f}$) of the signal based on the application and user requirement instead of delay and Doppler resolution. In this case, fractional delays occur with the same likelihood in OTFS systems as fractional Doppler shifts.

Moreover, the large bandwidth condition is not sufficient to ensure resolvable integer delays. In fact, the propagation environment also decides if the communication system have fractional delays or not. As a result, a generic paradigm for estimating and equalizing fractional delays and Doppler shifts is proposed in this paper.

A. Integer Delay & Fractional Doppler

In case of OTFS signal occupying large bandwidth with a small time duration integer delays and fractional Doppler shifts occur in the channel. The input-output relationship is derived as

$$\begin{aligned}\mathbf{y}&=\mathbf{H}_{\text{eff}}^{(\mathbf{i},\mathbf{f})}\mathbf{x}+\mathbf{w}\\&=(\mathbf{F}_N\otimes\mathbf{I}_M)\mathbf{H}^{(\mathbf{i},\mathbf{f})}(\mathbf{F}_N^H\otimes\mathbf{I}_M)\mathbf{x}+\mathbf{w},\end{aligned} \tag{11}$$

where $\mathbf{w}$, $\mathbf{H}_{\text{eff}}^{(\mathbf{i},\mathbf{f})}\in\mathbb{C}^{MN\times MN}$, and $\mathbf{H}^{(\mathbf{i},\mathbf{f})}\in\mathbb{C}^{MN\times MN}$ denote the additive white Gaussian noise (AWGN) vector with variance σ^2, the delay-Doppler, and the time equivalent channel matrices, respectively.[2]

Moreover, $\mathbf{H}^{(\mathbf{i},\mathbf{f})}$ in (11) can be expressed as

$$\mathbf{H}^{(\mathbf{i},\mathbf{f})}=\sum_{i=0}^{L-1}h_i\mathbf{\Pi}_{MN}^{l_i}\mathbf{\Delta}_{MN}^{(k_i+\kappa_i)}, \tag{12}$$

where $\mathbf{\Pi}_a^b$ is the $a\times a$ permutation matrix with $\Pi_a^b(l,k)=\delta([l-k]_a-b)$, and $\mathbf{\Delta}_a^c$ is the $a\times a$ diagonal matrix given as

$$\mathbf{\Delta}_a^c=\text{diag}\left[z_i^0,z_i^1,\ldots,z_i^{(a-1)}\right],\ \text{for}\ z_i=e^{\frac{j2\pi c}{a}}. \tag{13}$$

Consequently, the received signal becomes [24]

$$\begin{aligned}Y^{(\mathbf{i},\mathbf{f})}(l,k)=&\sum_{i=0}^{L-1}\sum_{q'=0}^{N-1}h_i\Gamma^{(i)}(l,k)\left(\frac{e^{-j2\pi(-q'-\kappa_i)}-1}{Ne^{-j\frac{2\pi}{N}(-q'-\kappa_i)}-N}\right)\\&X\left([l-l_i]_M,[k-k_i+q']_N\right)+W(l,k).\end{aligned} \tag{14}$$

[2]The channel matrix superscript denotes the type of delay and Doppler shifts, for instance, (i,f) and (f,i) stand for integer-fractional and fractional-integer delay and Doppler shifts, respectively.

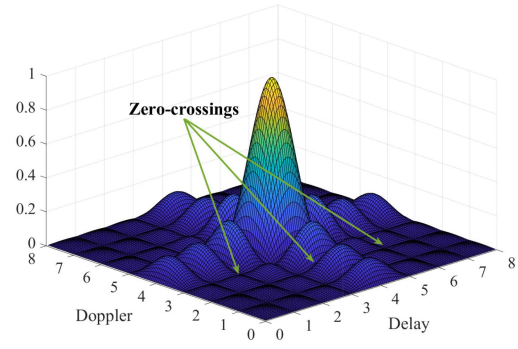

Fig. 1. Delay-Doppler domain OTFS waveform carrier (Pulsone).

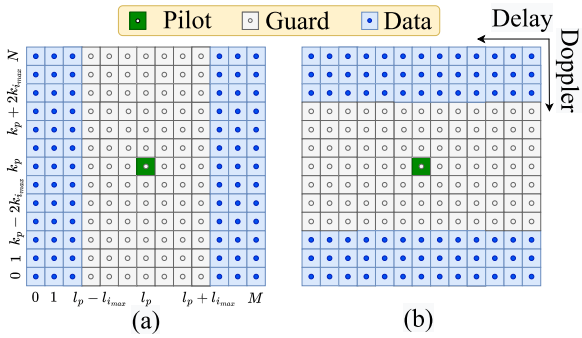

Fig. 2. Pilot and data symbols arrangement at the transmitter: (a) $(\mathbf{i},\mathbf{f})$ and (b) $(\mathbf{f},\mathbf{i})$.

where $\Gamma^{(i)}$ is a known phase term that denotes the type of prefix/suffix used and $W(l,k)$ represents the (l,k)-th element of noise matrix in delay-Doppler domain. The value of $\Gamma^i(l,k)$ depends on the prefix/suffix used [23]. In this paper, reduced-CP OTFS configuration is used, therefore $\Gamma^i(l,k)$ is found as

$$\Gamma^i(l,k)=e^{j2\pi\frac{k_i}{N}\frac{l-l_i}{M}}\begin{cases}1 & l_i\le l<M\\ e^{-j2\pi\frac{k}{N}} & 0\le l<l_i\end{cases}. \tag{15}$$

The new appearing term $\left(\frac{e^{-j2\pi(-q'-\kappa_i)}-1}{Ne^{-j\frac{2\pi}{N}(-q'-\kappa_i)}-N}\right)$ in (14) is due to fractional shifts of the two dimensional sinc pulse (shown in Fig. 1) in the Doppler dimension of the delay-Doppler grid causing IDI since sampling is no more at zero-crossings.

As seen from (14), the range of motion of the Doppler bins is the whole Doppler dimension as demonstrated by $q'=0,1,\ldots,N-1$. Therefore, the channel spreads throughout the Doppler dimension. Since the delay propagation is still integer, it would be sufficient to put guard as $l_p-l_i\le l_p\le l_p+l_i$ around the pilot in the delay dimension as depicted in Fig. 2(a). At the receiver side, the received symbols $Y_p^{(\mathbf{i},\mathbf{f})}(l,k)$ are used for channel estimation where

$$Y_p^{(\mathbf{i},\mathbf{f})}(l,k)=\begin{cases}Y^{(\mathbf{i},\mathbf{f})}(l,k), & \begin{matrix}l_p\le l\le l_p+l_{i_{\max}}\\ 0\le k\le N-1\end{matrix}\\ 0, & \text{otherwise}\end{cases}, \tag{16}$$

where $l_{i_{\max}}$ and $k_{i_{\max}}$ denote the maximum delay and Doppler spread, respectively.

B. Fractional Delay & Integer Doppler

Having fractional delays and integer Doppler shifts in the system is equivalent to having an integer delays channel but downsampled at the receiver side. So, the fractional delay channel matrix is a downsampled version of a larger matrix with integer delays. Specifically, the L tap fractional delay time-domain channel matrix can be given as

$$\mathbf{H}_{up}^{(\mathfrak{f},\mathbf{i})} = \sum_{i=0}^{L-1} h_i \mathbf{\Pi}_{\Omega MN}^{l_i} \mathbf{\Delta}_{\Omega MN}^{k_i}, \tag{17}$$

where Ω is the upsampling factor such that all the delay shifts are integers. Therefore, the upsampled received time-domain signal can be found as

$$\begin{aligned}\mathbf{r}_{up} &= \mathbf{H}_{up}^{(i,i)} \mathbf{F}_{\Omega MN}^{-1} \mathbf{A} (\mathbf{F}_{MN} \mathbf{s}) + \tilde{\mathbf{w}}_{up} \\ &= \underbrace{\mathbf{H}_{up}^{(i,i)} \mathbf{F}_{\Omega MN}^{-1} \mathbf{B}}_{\mathbf{G}^{(\mathfrak{f},\mathbf{i})}} (\mathbf{A}\mathbf{s}) + \tilde{\mathbf{w}}_{up},\end{aligned} \tag{18}$$

where $\tilde{\mathbf{w}}_{up}$ is the oversampled time-domain AWGN noise vector, $\mathbf{A}$ is the $\Omega MN \times MN$ zero padding matrix that is expressed as

$$\mathbf{A}(m,n) = \begin{cases} \mathbf{I}_N(m,n), & 0 \le n \le N-1 \\ 0, & \text{otherwise} \end{cases}, \tag{19}$$

$\mathbf{B} = \text{BlkDiag}(\mathbf{F}_{MN}, \mathbf{0}_{MN}, \ldots, \mathbf{0}_{MN})$ and $\mathbf{0}_{MN}$ is the $MN \times MN$ zeros matrix. Therefore, the time domain received signal can be computed from (18) as follows

$$\mathbf{r} = \mathbf{H}^{(\mathfrak{f},\mathbf{i})} \mathbf{s} + \tilde{\mathbf{w}}, \tag{20}$$

where $\mathbf{H}^{(\mathfrak{f},\mathbf{i})}(n', m') = \mathbf{G}^{(\mathfrak{f},\mathbf{i})}(n'\Omega, m')$ for $n' = 0, \ldots, MN-1$ and $m' = 0, \ldots, MN-1$. Then, the received signal in delay-Doppler domain is found as [24]

$$\begin{aligned}Y^{(\mathfrak{f},\mathbf{i})}(l,k) = \sum_{i=0}^{L-1} \sum_{q=0}^{M-1} h_i \Gamma^{(i)}(l,k) \left(\frac{e^{j2\pi(-q-\iota_i)} - 1}{M e^{j\frac{2\pi}{M}(-q-\iota_i)} - M} \right) \\ X\left([l - l_i + q]_M, [k - k_i]_N\right) + W(l,k).\end{aligned} \tag{21}$$

The new appearing term $\left(\frac{e^{j2\pi(-q-\iota_i)}-1}{M e^{j\frac{2\pi}{M}(-q-\iota_i)}-M} \right)$ in (21) is due to fractional shifts of the two dimensional sinc pulse in delay-Doppler domain in the delay directional causing inter-delay interference (IDeI) since these sinc pulses are no more sampled at their zero-crossings.

As indicated in (21), the fractional delay shifts induce spreading of all the symbols in delay dimension. Thus, to avoid the IDeI the pilot arrangement is chosen to be as shown in Fig. 2(b). At the receiver side, the received symbols $Y_p^{(\mathfrak{f},\mathbf{i})}(l,k)$ are used for channel estimation where

$$Y_p^{(\mathfrak{f},\mathbf{i})}(l,k) = \begin{cases} Y^{(\mathfrak{f},\mathbf{i})}(l,k), & 0 \le l \le M-1 \\ & k_p - k_{i_{\max}} \le k \le k_p + k_{i_{\max}} \\ 0, & \text{otherwise} \end{cases}. \tag{22}$$

IV. Preliminaries

First, we introduce the lemma on the self-duality of the pulsone between time and frequency domains. Then, we introduce the lemma on the pulsone being shape-invariant to delay and Doppler shifts.

Lemma 1: A pulsone is self-dual between time and frequency, such that applying Fourier transform to a pulsone results in a pulsone as well. The time domain pulsone can be seen as a frequency modulated pulse train, thus it is expressed as

$$s_p(n) = \sum_{k'=0}^{N-1} \delta\left(n - (l_p + k'M)\right) e^{j2\pi \frac{k_p n}{MN}}. \tag{23}$$

The frequency representation of the pulsone can be found by applying DFT operation to (23) as follows

$$S_p(f) = \mathcal{F}\{\mathbf{s}_p\} = \sum_{n=0}^{MN-1} s_p(n) e^{\frac{-j2\pi f n}{MN}}. \tag{24}$$

The frequency shifting property states that the Fourier transform of the modulated signal in time is the shifted version of its Fourier transforms in frequency [25]. Then, we find

$$\begin{aligned}S_p(f) &= \sum_{k'=0}^{N-1} \mathcal{F}\{\delta\left(n - (l_p + k'M)\right)\} * \delta(f - k_p) \\ &= \sum_{k'=0}^{N-1} e^{\frac{-j2\pi(f-k_p)(l_p+k'M)}{MN}} = e^{\frac{-j2\pi l_p (f-k_p)}{MN}} \sum_{k'=0}^{N-1} e^{\frac{-j2\pi k'(f-k_p)}{N}}.\end{aligned} \tag{25}$$

The second term in (25) is periodic over $f \in [0, MN-1]$, with period N as follows

$$\sum_{k'=0}^{N-1} e^{\frac{-j2\pi k'(f-k_p)}{N}} = \sum_{k'=0}^{N-1} e^{\frac{-j2\pi k'([f]_N - k_p)}{N}}. \tag{26}$$

Also, for $f \in [0, N-1]$ the summation in (26) becomes equivalent to the DFT which results in

$$\sum_{k'=0}^{N-1} e^{\frac{-j2\pi k'(f-k_p)}{N}} = \delta\left(f - k_p\right). \tag{27}$$

Then, the frequency representation of a pulsone in (25) becomes

$$S_p(f) = \sum_{l'=0}^{M-1} \delta\left(f - (k_p + l'N)\right) e^{\frac{-j2\pi l_p (f-k_p)}{MN}}. \tag{28}$$

As seen from (28), *the frequency representation of a pulsone is indeed a pulsone where k_p becomes the amount of the shift of the pulse train and l_p becomes the frequency of the modulator tone in frequency domain, so, τ and ν are interchangeable between time and frequency domains.*[3]

Lemma 2: The OTFS waveform carrier or pulsone holds its shape under the operations of time delay and Doppler shifts, where it extends quasi-periodically in the delay-Doppler

[3]The pilot-pulsone location in delay-Doppler domain does not affect the performance of the channel estimation. Then, for simplicity it is assumed that $l_p = 0$ and $k_p = 0$ for the rest of this paper.

grid. Here, the cases of integer-delay fractional-Doppler and fractional-delay integer-Doppler are considered as follows

Case 1: In the case of integer-delay ($\iota_i = 0$) fractional-Doppler channel and if $M > l_i$, after passing through a doubly-dispersive channel, the received signal can be found according to (7) as

$$r_p^{(\mathbf{i},\mathbf{f})}(n) = \sum_{k'=0}^{N-1}\sum_{i=0}^{L-1} h_i \delta\left(n-(l_i+k'M)\right) e^{j2\pi k' \frac{(k_i+\kappa_i)}{N}}. \quad (29)$$

Consider the α-th power of $r_p^{(\mathbf{i},\mathbf{f})}(n)$ given by

$$[r_p^{(\mathbf{i},\mathbf{f})}(n)]^{\alpha} = \left[\sum_{k'=0}^{N-1}\sum_{i=0}^{L-1} h_i \delta\left(n-(l_i+k'M)\right) e^{j2\pi k' \frac{(k_i+\kappa_i)}{N}}\right]^{\alpha}. \quad (30)$$

Lemma 2 states that for $M > l_i$, there is no inter-symbol interference between $r_p(n)^{(\mathbf{i},\mathbf{f})}$ samples. Thus, powers of $[r_p^{(\mathbf{i},\mathbf{f})}(n)]^{\alpha}$ can be found by taking the power of each element ignoring the double summation in (30). Therefore, we find

$$[r_p^{(\mathbf{i},\mathbf{f})}(n)]^{\alpha} = \sum_{k'=0}^{N-1}\sum_{i=0}^{L-1} h_i^{\alpha} \delta\left(n-(l_i+k'M)\right) e^{j2\pi k' \frac{\alpha(k_i+\kappa_i)}{N}}. \quad (31)$$

Case 2: In the case of fractional-delay integer-Doppler ($\kappa_i = 0$) channel and if $M > l_i$, after passing through a doubly-dispersive channel, the received time domain signal $r_p^{(\mathbf{f},\mathbf{i})}(n)$ can be found as follows

$$r_p^{(\mathbf{f},\mathbf{i})}(n) = \sum_{k'=0}^{N-1}\sum_{i=0}^{L-1} h_i \delta\left(n-(l_i+\iota_i+k'M)\right) e^{\frac{j2\pi k' k_i}{N}}. \quad (32)$$

Using Lemma 1, it is found that the transmitted pilot impulse is self-dual between time and frequency, such that applying Fourier transform to it results in another OTFS carrier. However, the only change is that the delay and Doppler shifts will exchange places as shown in (25). Therefore, the frequency representation $R_p(f) = \mathcal{F}\{r_p(n)\}$ of the whole received time pilot signal in (32) can be found based on (28) as

$$R_p^{(\mathbf{f},\mathbf{i})}(f) = \sum_{l'=0}^{M-1}\sum_{i=0}^{L-1} h_i \delta\left(f-k_i-l'N\right) e^{\frac{-j2\pi(l_i+\iota_i)f}{MN}}. \quad (33)$$

Consider the α-th power of $R_p^{(\mathbf{f},\mathbf{i})}(f)$ given by

$$[R_p^{(\mathbf{f},\mathbf{i})}(f)]^{\alpha} = \left[\sum_{l'=0}^{M-1}\sum_{i=0}^{L-1} h_i^{\alpha} \delta\left(f-k_i-l'N\right) e^{\frac{-j2\pi(l_i+\iota_i)f}{MN}}\right]^{\alpha}. \quad (34)$$

Lemma 2 states that for $M > l_i$, there is no inter-symbol interference between $R_p(f)^{(\mathbf{f},\mathbf{i})}$ samples. Thus, powers of $[R_p^{(\mathbf{f},\mathbf{i})}(f)]^{\alpha}$ can be found by taking the power of each element ignoring the double summation in (34). Therefore, we find

$$[R_p^{(\mathbf{f},\mathbf{i})}(f)]^{\alpha} = \sum_{l'=0}^{M-1}\sum_{i=0}^{L-1} h_i^{\alpha} \delta\left(f-k_i-l'N\right) e^{\frac{-j2\pi\alpha(l_i+\iota_i)f}{MN}}. \quad (35)$$

Fig. 3 summarizes both Lemmas 1 and 2. For instance, Fig. 3(a) depicts a time-domain pulsone $s_p(t)$ while Fig. 3(b) illustrates its frequency representation $S_p(f)$. It is clearly seen that the frequency representation of a pulsone is indeed another pulsone and that the delay and Doppler shifts are interchanged between time and frequency domains as stated in Lemma 1. This is also the case between Fig. 3(c)–(d) and (e)–(f). On the other hand, raising the pulsone to power $\alpha = 2$, results in another pulsone $[s_p(t)]^2$ having the same delay shift l_i and αk_i Doppler shift as shown in Fig. 3(c). Additionally, raising the frequency domain pulsone to power $\alpha = 2$, as shown in Fig. 3(f), results in pulsone $\mathcal{F}^{-1}\{[S_p(f)]^2\}$ having the same Doppler shift k_i and αl_i delay shift as shown in Fig. 3(e), thus proving Lemma 2.

V. Proposed Channel Estimation and Equalization Framework

In this section, we provide a paradigm for estimating and equalizing fractional doubly-dispersive channels. The analysis is divided into two parts. Specifically, in the first part we show that for a chosen α_{opt} fractional delay and Doppler shifts can be changed to integers ones in delay Doppler domain. Based on these findings, in the second part, we propose a framework to estimate the fractional delay and Doppler shifts without the need of finding α_{opt}. Note that the main scope of this paper is estimating the fractional delay and Doppler shifts. Then, the estimation of the complex gain of each channel tap is not covered since it is studied in [15], [16], [17], [18], [19], [20], [21], [22], [26].

A. Fractional Doppler Shift Estimation

For simplicity, the proposed method is explained first considering a single-tap fractional Doppler channel. Then, it is generalized for any doubly-dispersive channel.

1) One-tap Channel: To estimate fractional Doppler shifts in the channel, the received $Y_p^{(\mathbf{i},\mathbf{f})}(l,k)$ signal in (16) is exploited. In fact, $Y_p^{(\mathbf{i},\mathbf{f})}(l,k)$ is delay-Doppler representation of a pulsone that passed through a one-tap doubly-dispersive channel which is given by (29). Lemma 2 states that the powers of $[r_p^{(\mathbf{i},\mathbf{f})}(n)]^{\alpha}$ can be found as

$$[r_p^{(\mathbf{i},\mathbf{f})}(n)]^{\alpha} = \sum_{k'=0}^{N-1} h_i^{\alpha} \delta\left(n-(l_i+k'M)\right) e^{j2\pi k' \frac{\alpha(k_i+\kappa_i)}{N}}. \quad (36)$$

Note that the term h_i^{α} in (36) will cause the term to vanish for $\alpha >> 1$, such that

$$\lim_{\alpha\to\infty}(h_i^{\alpha}) = 0; \text{ for } |h_i| < 1. \quad (37)$$

Therefore, instead of taking the powers of $r_p^{(\mathbf{i},\mathbf{f})}(n)$, we consider the powers of the phase of the received signal $\angle r_p^{(\mathbf{i},\mathbf{f})}(n)$ since it is the one containing the Doppler shift information. Then, we find

$$[r_p^{(\mathbf{i},\mathbf{f})}(n)]^{\alpha} = |r_p^{(\mathbf{i},\mathbf{f})}(n)| \cdot [\angle r_p^{(\mathbf{i},\mathbf{f})}(n)]^{\alpha}$$

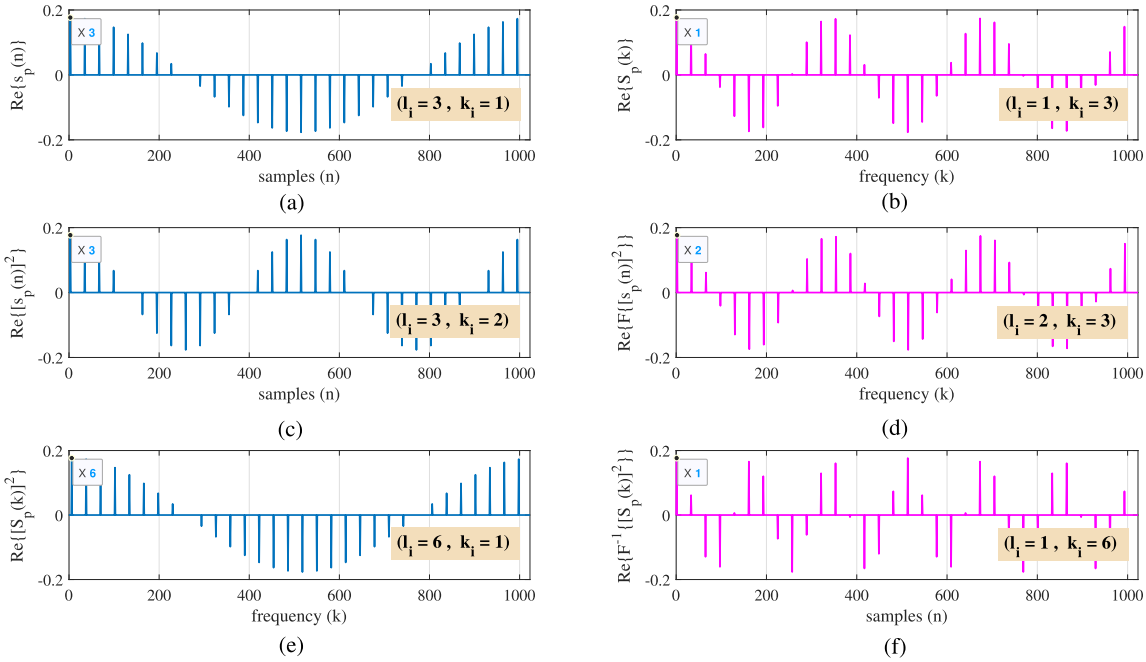

Fig. 3. Pulsone properties: (a) $s_p(t)$; (b) $S_p(f) = \mathcal{F}\{s_p(t)\}$; (c) $[s_p(t)]^2$; (d) $\mathcal{F}\{[s_p(t)]^2\}$; (e) $[S_p(f)]^2$; (f) $\mathcal{F}^{-1}\{[S_p(f)]^2\}$.

$$= \sum_{k'=0}^{N-1} |h_i| e^{\alpha\theta_i} \delta\left(n - (l_i + k'M)\right) e^{j2\pi k' \frac{\alpha(k_i+\kappa_i)}{N}}, \tag{38}$$

where $\theta_i = \angle h_i$. Consequently, the delay-Doppler representation of $[r_p^{(\mathbf{i},\mathbf{f})}(n)]^\alpha$ is found as

$$Y_{p,\alpha}^{(\mathbf{i},\mathbf{f})}(l,k) = \sum_{q'=0}^{N-1} |h_i| e^{\alpha\theta_i} \Gamma^{(i)}(l,k) \left(\frac{e^{-j2\pi(-q'-\alpha\kappa_i)} - 1}{N e^{-j\frac{2\pi}{N}(-q'-\alpha\kappa_i)} - N} \right) \delta\left([l-l_i]_M, [k-\alpha k_i + q']_N\right). \tag{39}$$

As seen from (36) and (39), it is possible to convert the fractional Doppler shift into integer just by ensuring the following condition

$$\alpha_{\text{opt}}\kappa_i \in \mathbb{Z}; \quad \alpha = 1, 2, \ldots, \alpha_{\max}. \tag{40}$$

Then, we have

$$\begin{aligned} &Y_{p,\alpha}^{(\mathbf{i},\mathbf{f})}(l,k) \\ &= |h_i| e^{\alpha\theta_i} \Gamma^{(i)}(l,k) \delta(q' + \alpha\kappa_i) s\delta([l-l_i]_M, [k-\alpha k_i + q']_N) \\ &= |h_i| e^{\alpha\theta_i} \Gamma^{(i)}(l,k) \delta\left([l-l_i]_M, [k-\alpha(k_i+\kappa_i)]_N\right). \end{aligned} \tag{41}$$

From (41), it is concluded that trying different α values until the condition in (40) is satisfied, can give us the exact integer and fractional Doppler shifts as follows

$$[\alpha_{\text{opt}}(k_i + \kappa_i)]_M = \gamma \in \mathbb{Z}. \tag{42}$$

2) Multi-tap Channel: In the case of multi-tap doubly-dispersive channels with fractional Doppler shifts, the same process in the one-tap case can be followed. The only difference is that all Doppler bins are monitored in parallel for each value of α. For instance, the first tap can turn to integer for $\alpha_{\text{opt}} = 2$, where the second tap becomes integer at $\alpha_{\text{opt}} = 5$. The delay-Doppler representation of the received pilot signal is given by

$$\begin{aligned} &Y_{p,\alpha}^{(\mathbf{i},\mathbf{f})}(l,k) \\ &= \sum_{i=1}^{L} |h_i| e^{\alpha\theta_i} \Gamma^{(i)}(l,k) \delta\left([l-l_i]_M, [k-\alpha(k_i+\kappa_i)]_N\right). \end{aligned} \tag{43}$$

Algorithm 1: The Proposed Fractional Doppler Channel Estimation Framework.

Input: $\mathbf{Y}^{(\mathbf{i},\mathbf{f})}$
Output: $k_i + \kappa_i$ for $i \in [0, L-1]$.
Extract $\mathbf{Y}_p^{(\mathbf{i},\mathbf{f})}$ from $\mathbf{Y}^{(\mathbf{i},\mathbf{f})}$ as in (16).
Convert $\mathbf{Y}_p^{(\mathbf{i},\mathbf{f})}$ from delay-Doppler to time domain $r_p^{(\mathbf{i},\mathbf{f})}(n)$ (29).
Estimate the integer and fractional Doppler shift induced by the channel:
  Input: Time domain pilot signal $r_p^{(\mathbf{i},\mathbf{f})}(n)$ and maximum power value α_{max}.
  Output: $k_i + \kappa_i \quad \forall i \in (0, L-1)$.
  for $i = 0, 1, \ldots, L-1$ **do**
    while $\alpha \leq \alpha_{max}$ **do**
      Compute $[r_p^{(\mathbf{i},\mathbf{f})}(n)]^\alpha$ as in (38).
      Convert $[r_p^{(\mathbf{i},\mathbf{f})}(n)]^\alpha$ to delay-Doppler domain $Y_{p,\alpha}^{(\mathbf{i},\mathbf{f})}(l,k)$ (41).
      $\mathcal{K}_{i,\alpha} = \arg\max_k(|Y_{p,\alpha}^{(\mathbf{i},\mathbf{f})}(l_i,k)|)$.
      $\mathcal{D}_{i,\alpha} = \mathcal{K}_{i,\alpha} - \mathcal{K}_{i,\alpha-1}$.
    $k_i + \kappa_i = \mathrm{E}_\alpha\{\mathcal{D}_{i,\alpha}\}$.

B. Fractional Doppler Channel Estimation Framework

In the method proposed in Section V-A finding α_{opt} is a requirement. To overcome this constraint, we propose an enhanced algorithm to find all integer and fractional Doppler shifts at once. Initially, $Y_{p,\alpha}^{(\mathbf{i},\mathbf{f})}(l,k)$ is computed for $\alpha = 1,\ldots,\alpha_{\max}$. Then, for each α and delay l_i values, the Doppler grid index of the highest bin (in terms of power) is found as follows

$$\mathcal{K}_{i,\alpha} = \arg\max_{k}(|Y_{p,\alpha}^{(\mathbf{i},\mathbf{f})}(l_i,k)|). \tag{44}$$

After that, the difference between each successive $\mathcal{K}_{i,\alpha}$ is calculated as follows

$$\mathcal{D}_{i,\alpha} = \mathcal{K}_{i,\alpha} - \mathcal{K}_{i,\alpha-1}. \tag{45}$$

Finally, the integer and fractional Doppler shifts are found by taking the mean of the differences as follows

$$k_i + \kappa_i = \mathrm{E}_{\alpha}\{\mathcal{D}_{i,\alpha}\}. \tag{46}$$

Algorithm 1 summarizes the proposed fractional Doppler channel estimation framework.

C. Fractional Delay Shift Estimation

For simplicity, we first explain the proposed method considering a single tap with fractional delay shift, and then, the proposed method is generalized for any doubly-dispersive channel. To estimate fractional delay shifts in the channel, the received $Y_p^{(\mathbf{f},\mathbf{i})}(l,k)$ signal in (22) is exploited. Using Lemma 1, the frequency representation of the whole received time pilot signal can be found based on (28) as

$$R_p^{(\mathbf{f},\mathbf{i})}(f) = \sum_{l'=0}^{M-1} h_i \delta\left(f - k_i - l'N\right) e^{\frac{-j2\pi(l_i+\iota_i)f}{MN}}. \tag{47}$$

1) One-tap Channel: In the method proposed in Section V-A finding α_{opt} is a requirement. To overcome this constraint, To estimate fractional delay shifts in the channel, the same steps applied in Section V-A can be followed here but on the frequency representation of the received pilot signal. Assuming a single tap channel, the α-th power of $R_p^{(\mathbf{f},\mathbf{i})}(f)$ given by

$$[R_p^{(\mathbf{f},\mathbf{i})}(f)]^{\alpha} = \sum_{l'=0}^{M-1} |h_i| e^{\alpha\theta_i} \delta\left(f - k_i - l'N\right) e^{\frac{-j2\pi\alpha(l_i+\iota_i)f}{MN}}. \tag{48}$$

Consequently, the time-domain single of $[R_p^{(\mathbf{f},\mathbf{i})}(f)]^{\alpha}$ can be found by taking the inverse DFT of (48) as follows

$$\begin{aligned} r_{p,\alpha}^{(\mathbf{f},\mathbf{i})}(n) &= \mathcal{F}^{-1}\left\{R_p^{(\mathbf{f},\mathbf{i})}(f)\right\} \\ &= \sum_{k'=0}^{N-1} |h_i| \delta\left(n - (\alpha(l_i+\iota_i) + k'M)\right) e^{\frac{j2\pi k' k_i}{N}}. \end{aligned} \tag{49}$$

Furthermore, the delay-Doppler representation of $r_{p,\alpha}^{(\mathbf{f},\mathbf{i})}(n)$ is found as

$$Y_{p,\alpha}^{(\mathbf{f},\mathbf{i})}(l,k) = \sum_{q=0}^{N-1} |h_i| e^{\alpha\theta_i} \Gamma^{(i)}(l,k) \left(\frac{e^{j2\pi(-q-\alpha\iota_i)} - 1}{M e^{j\frac{2\pi}{M}(-q-\alpha\iota_i)} - M}\right)$$

Algorithm 2: The Proposed Fractional Delay Shift Estimation Framework.

Input: $\mathrm{Y}^{(\mathbf{f},\mathbf{i})}$
Output: $l_i + \iota_i$ for $i \in [0, L-1]$.
Extract $\mathbf{Y}_p^{(\mathbf{f},\mathbf{i})}$ from $\mathbf{Y}^{(\mathbf{f},\mathbf{i})}$ as in (22).
Convert $\mathbf{Y}_p^{(\mathbf{f},\mathbf{i})}$ from delay-Doppler to time domain $r_p^{(\mathbf{f},\mathbf{i})}(n)$ (32).
Convert $r_p^{(\mathbf{f},\mathbf{i})}(n)$ from time to frequency domain $R_p^{(\mathbf{f},\mathbf{i})}(f)$ (47).
Estimate the integer and fractional delay shift induced by the channel:
  Input: Time domain pilot signal $R_p^{(\mathbf{f},\mathbf{i})}(n)$ and maximum power value α_{max}.
  Output: $l_i + \iota_i \quad \forall i \in (0, L-1)$.
  for $i = 0, 1, \ldots, L-1$ **do**
    while $\alpha \le \alpha_{max}$ **do**
      Compute $[R_p^{(\mathbf{f},\mathbf{i})}(f)]^{\alpha}$ as in (48).
      Convert $[R_p^{(\mathbf{f},\mathbf{i})}(f)]^{\alpha}$ to time domain $r_{p,\alpha}^{(\mathbf{f},\mathbf{i})}(n) = \mathcal{F}^{-1}\left\{R_p^{(\mathbf{f},\mathbf{i})}(f)\right\}$ (49).
      Convert $r_{p,\alpha}^{(\mathbf{f},\mathbf{i})}(n)$ to delay-Doppler domain $Y_{p,\alpha}^{(\mathbf{f},\mathbf{i})}(l,k)$ (52).
      $\mathcal{L}_{i,\alpha} = \arg\max_{l}(|Y_{p,\alpha}^{(\mathbf{f},\mathbf{i})}(l,k_i)|)$.
      $\mathcal{D}_{i,\alpha} = \mathcal{L}_{i,\alpha} - \mathcal{L}_{i,\alpha-1}$.
    $l_i + \iota_i = \mathrm{E}_{\alpha}\{\mathcal{D}_{i,\alpha}\}$.

$$\delta\left([l - \alpha l_i + q]_M, [k - k_i]_N\right). \tag{50}$$

As seen from (49) and (50), it is possible to convert the fractional delay shift into an integer just by ensuring the following condition

$$\alpha_{\text{opt}}\iota_i \in \mathbb{Z}. \tag{51}$$

Then, we have

$$\begin{aligned} &Y_{p,\alpha}^{(\mathbf{f},\mathbf{i})}(l,k) \\ &= |h_i| e^{\alpha\theta_i} \Gamma^{(i)}(l,k) \delta(q+\alpha\iota_i) \delta\left([l - \alpha l_i + q]_M, [k - k_i]_N\right) \\ &= |h_i| e^{\alpha\theta_i} \Gamma^{(i)}(l,k) \delta\left([l - \alpha(l_i+\iota_i)]_M, [k - k_i]_N\right). \end{aligned} \tag{52}$$

It is concluded from (52) that trying different α until the condition in (51) fulfilled can give us the exact integer and fractional delay shift.

2) Multi-tap Channel: In the case of multi-tap channels with fractional delay shifts, all Doppler bins are processed in parallel for each value of α. The delay-Doppler representation of the received pilot signal is given by

$$\begin{aligned} &Y_{p,\alpha}^{(\mathbf{f},\mathbf{i})}(l,k) \\ &= \sum_{i=1}^{L} |h_i| e^{\alpha\theta_i} \Gamma^{(i)}(l,k) \delta\left([l - \alpha(l_i+\iota_i)]_M, [k - k_i]_N\right). \end{aligned} \tag{53}$$

D. Fractional Delay Channel Estimation Framework

Similar to estimating fractional Doppler shifts, in the approach proposed in Section V-C finding α_{opt} is a needed. Thus, to overcome this constraint we propose an enhanced algorithm to find all integer and fractional delay shifts at once. Initially, $Y_{p,\alpha}^{(\mathbf{f},\mathbf{i})}(l,k)$ is computed for $\alpha = 1,\ldots,\alpha_{\max}$. Then, for each α and Doppler shift k_i values, the Doppler index of the max power bin is found as

$$\mathcal{L}_{i,\alpha} = \arg\max_{l}(|Y_{p,\alpha}^{(\mathbf{f},\mathbf{i})}(l,k_i)|). \tag{54}$$

After that, the difference between each successive $\mathcal{L}_{i,\alpha}$ is calculated as follows

$$\mathcal{D}_{i,\alpha} = \mathcal{L}_{i,\alpha} - \mathcal{L}_{i,\alpha-1}. \tag{55}$$

Finally, the integer and fractional Doppler shifts are found by taking the mean of the differences as follows

$$l_i + \iota_i = \mathrm{E}_{\alpha}\{\mathcal{D}_{i,\alpha}\}. \tag{56}$$

Algorithm 2 summarizes the proposed fractional delay channel estimation framework.

E. Joint Fractional Delay and Doppler Channel Estimation Framework

Since delays and Doppler shifts are uncoupled, they can be estimated separately by compiling both Algorithms 1 and 2, which do not need to neither determine α_{opt} nor verify the condition $(\alpha\kappa_j, \alpha\iota_j) \in \mathbb{Z}$. In the proposed algorithm, the only design parameter is $\alpha_{\max}$ (not α_{opt}) as shown by Fig. 5, which will be investigated in detail in the simulation section. Fig. 5 helps to determine $\alpha_{\max}$ based on the SNR of the pilot transmitted. Specifically, the design parameter $\alpha_{\max}$ is selected based on three criteria:

- *Pilot power (SNR$_p$):* based on the transmitted pilot power, the upper limit of α is found. For instance, as depicted in Fig. 5(a), for SNR$_p$ = 30 dB the upper limit of α before the performance decreases is $\alpha_{opt} = 22$.
- *Performance:* in case that high accuracy estimation is needed, then $\alpha_{\max}$ is set up to be $\alpha_{\max} = \alpha_{opt}$. However, this will be computationally expensive to execute.
- *Computational complexity:* in the case of computationally limited devices or low-latency communication where very high accuracy is not needed, then $\alpha_{\max}$ can be set from Fig. 8 based on the required computational complexity.

Here is a simple example to illustrate how the algorithm works. Consider a single tap channel with $l_0 = 0$ and $k_0 + \kappa_0 = 1.12$. Ignoring the received noiseless pilot is given as

$$Y_{p,\alpha}(l,k) = |h_0|e^{\alpha\theta_0}\Gamma^{(0)}(l,k)\delta\left([l]_M, [k-1.12\alpha]_N\right). \tag{57}$$

Assuming that SNR$_p$ = 35 dB, which is practical, the upper limit is given in Fig. 5(a) as $\alpha_{opt} = 38$.

In the event that high accuracy estimation (performance) is needed, then:

1) Choose $\alpha_{\max} = \alpha_{opt} = 38$.
2) Compute $Y_{p,\alpha}$ for each $\alpha = 1, 2, \ldots, 36$.

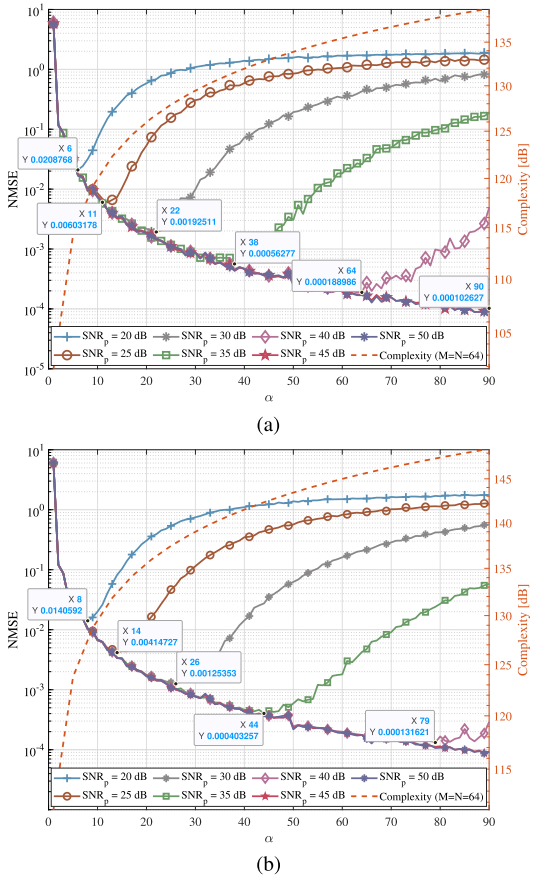

Fig. 4. NMSE vs α analysis. (a) Fractional Doppler case. (b) Fractional delay case.

3) Find the Doppler bin index of the peak of the tap for each α. Then put the result in a vector $\mathcal{K}_0 = [1,2,3,4,15,0,8,9,10,\ldots,35,36,37,38,39,40]$. Note that the fifth and sixth elements of $\mathcal{K}_0$ are erroneous (should be 6 and 7 instead of 15 and 0, respectively), we did that to show the noise effect.
4) Compute the difference vector as follows $\mathcal{D}_0 = \mathcal{K}_0(l+1) - \mathcal{K}_0(l) = [1,1,1,11,-15,1,1,\ldots,1,1,1,1]$.
5) Estimate the Doppler shift $\hat{k}_0 + \hat{\kappa}_0 = \mathrm{E}\{\mathcal{D}_0\} = 1.114$.

The MSE of the estimator is: $\mathrm{MSE}(\hat{k}_0 + \hat{\kappa}_0) = 3.25 \cdot 10^{-5}$. In cases of low computational complexity requirements, $\alpha_{\max}$ could be set to a lower value, giving up some of the performance. For instance, for $\alpha_{\max} = 20$ the MSE of the estimator is: $\mathrm{MSE}(\hat{k}_0 + \hat{\kappa}_0) = 2.16 \cdot 10^{-4}$.

VI. Performance Analysis

A. Cramer-Rao Lower Bound

We will compare the performance of our proposed algorithm with that of CRLB, which is a computational technique that uses the Fisher information matrix for maximum performance benchmark. First, CRLB will be derived separately for the fractional delay and Doppler coefficients ι and κ, respectively. For this, the received delay-Doppler domain signals can be written as [21]

$$Y(l,k) = U(l,k) + W(l,k), \tag{58}$$

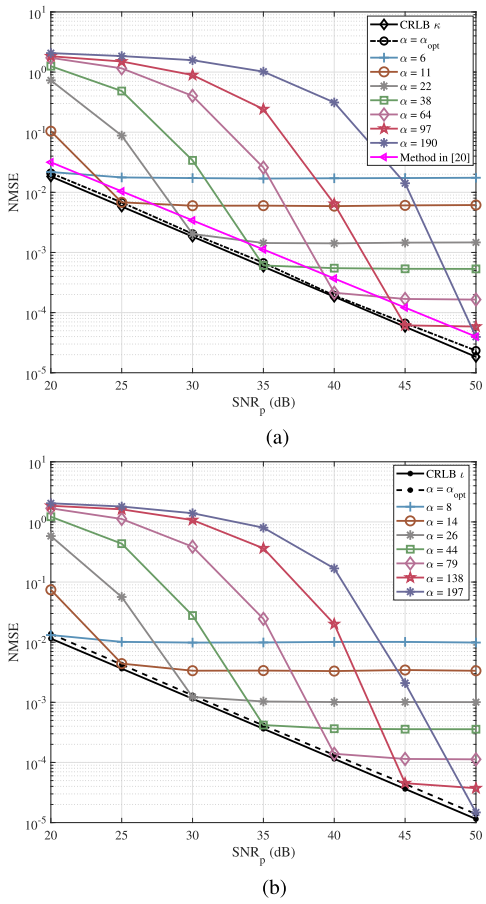

Fig. 5. NMSE vs SNR$_p$ analysis. (a) Fractional Doppler case. (b) Fractional delay case.

where $U(l,k)$ represents the received signal without noise effect and will be used for the Fisher information matrix calculation. For the fractional Doppler and fractional delay cases $U(l,k)$ can be respectively given by

$$U^{(\mathbf{i},\mathbf{f})}(l,k) = \sum_{i=1}^{L}\sum_{q'=0}^{N-1} h_i \Gamma^{(i)}(l,k)\left(\frac{e^{-j2\pi(-q'-\kappa_i)}-1}{Ne^{-j\frac{2\pi}{N}(-q'-\kappa_i)}-N}\right) X\left([l-l_i]_M, [k-k_i+q']_N\right), \tag{59}$$

and

$$U^{(\mathbf{f},\mathbf{i})}(l,k) = \sum_{i=1}^{L}\sum_{q=0}^{M-1} h_i \Gamma^{(i)}(l,k)\left(\frac{e^{j2\pi(-q-\iota_i)}-1}{Me^{j\frac{2\pi}{M}(-q-\iota_i)}-M}\right) X\left([l-l_i+q]_M, [k-k_i]_N\right). \tag{60}$$

In the case of fractional Doppler channel, we define the $\boldsymbol{\theta} = [\kappa_1, \kappa_2, \ldots \kappa_L]^T$ (or $\boldsymbol{\theta} = [\iota_1, \iota_2, \ldots \iota_L]^T$ for the fractional delay channel) for the derivation of CRLB. The j-th diagonal element of inverse of the Fisher information matrix is j-th element of CRLB which is given as

$$\boldsymbol{\theta}_j^{\text{CRLB}} = [\mathbf{I}^{-1}(\boldsymbol{\theta})]_{jj}, \tag{61}$$

where the $L \times L$ matrix $\mathbf{I}(\boldsymbol{\theta})$ represents the Fisher information matrix. The (i,j)-th element of $\mathbf{I}(\boldsymbol{\theta})$ can be found as follows

$$[\boldsymbol{I}(\boldsymbol{\theta})]_{ij} = -\mathbb{E}\left[\frac{\partial^2 \ln p(\boldsymbol{y};\boldsymbol{\theta})}{\partial\theta_i \partial\theta_j}\right], \tag{62}$$

where $i = 1,2,\ldots,L$, $j = 1,2,\ldots,L$, $\boldsymbol{y} = \text{vec}(\mathbf{Y})$, and the expectation is taken with respect to $p(\boldsymbol{y};\boldsymbol{\theta})$. From (57), the received signal $Y(l,k)$ follows the same distribution as the noise. Assuming the noise to be AWGN the joint probability density function (PDF) of $p(\boldsymbol{y};\boldsymbol{\theta})$ can be expressed as

$$p(\boldsymbol{y};\boldsymbol{\theta}) = \prod_{z=0}^{Z-1} \frac{1}{\sigma\sqrt{2\pi}} e^{-\frac{1}{2}\left(\frac{Y_z-\mu_z}{\sigma}\right)^2}, \tag{63}$$

where $\mu_z = U_z$ and Z denotes the total number of received samples used to estimate the channel which is equivalent to the guard symbols. Next, the likelihood function to convert the product of probability into a summation, and $\ln p(\boldsymbol{y};\boldsymbol{\theta})$ can be represented as

$$\ln p(\boldsymbol{y};\boldsymbol{\theta}) = -\frac{Z}{2}\ln\left(2\pi\sigma^2\right) - \frac{1}{2\sigma^2}\sum_{z=0}^{Z-1}|Y_z - U_z|^2, \tag{64}$$

where Y_z and U_z denote the z-th element of vectorized form of $\mathbf{Y}$ and $\mathbf{U}$. Hence (62) can be rewritten as

$$[\boldsymbol{I}(\boldsymbol{\theta})]_{ij} = \frac{1}{2\sigma^2}\sum_{z=0}^{Z-1}\left[-\frac{\partial u_z}{\partial\theta_i}\frac{\partial u_z^*}{\partial\theta_j} - \frac{\partial u_z^*}{\partial\theta_i}\frac{\partial u_z}{\partial\theta_j}\right]. \tag{65}$$

To calculate the Fisher information matrix, U must be differentiated with respect to the variables κ and ι to be estimated. The derivative for the Fisher information matrix with respect to κ is given by (66) shown at the bottom of the next page and the derivative with respect to ι is given by (67) shown at the bottom of the next page.[4]

For the performance analysis of the proposed algorithm in terms of normalized mean square error (NMSE), CRLB should be normalized separately with respect to fractional delay and Doppler shift as follows

$$\hat{\boldsymbol{\kappa}}_{\text{bound}} = \frac{\sum_{j=1}^{L}\theta_j^{CRLB}}{\|\boldsymbol{\kappa}_{\boldsymbol{\theta}}\|_2^2}, \quad \hat{\boldsymbol{\iota}}_{\text{bound}} = \frac{\sum_{j=1}^{L}\theta_j^{CRLB}}{\|\boldsymbol{\iota}_{\boldsymbol{\theta}}\|_2^2}, \tag{68}$$

where $\boldsymbol{\kappa}_{\boldsymbol{\theta}} = [\kappa_1, \kappa_2, \ldots, \kappa_L]^T$ and $\boldsymbol{\iota}_{\boldsymbol{\theta}} = [\iota_1, \iota_2, \ldots, \iota_L]^T$.

B. Computational Complexity Analysis

In this section, computational complexity analysis of the proposed methods is examined in terms of number of complex multiplications. The complexity of complex DFT is computed using the Split-Radix algorithm as in [27].

1) Fractional Doppler Channel Estimation: The computational complexity of the fractional Doppler channel estimation framework can be computed directly from Algorithm 1. For instance, in *step 2* the delay-Doppler domain symbols are converted back to the time domain with the complexity

[4]The derived CRLB is relaxed since the non-zero elements are assumed to be known.

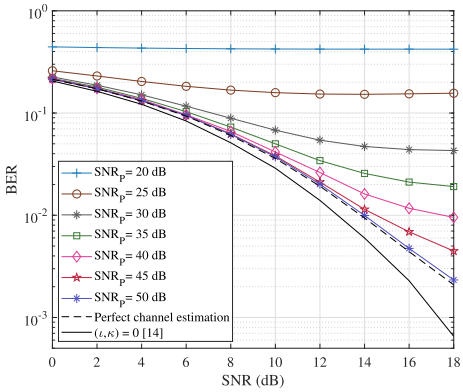

Fig. 6. BER vs SNR_p analysis.

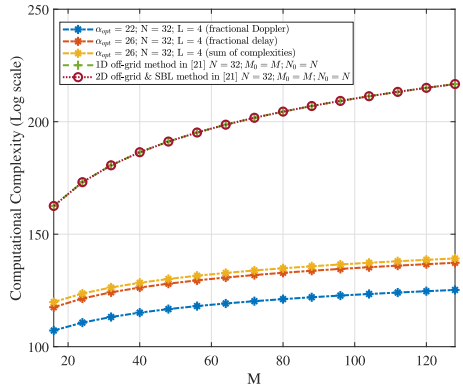

Fig. 7. Computational complexity analysis.

$\mathcal{O}_2^1 = MN\log(N)$ which is valid for rectangular pulse shaping [28]. *Step 6* raises the powers of the received time samples which is of complexity $\mathcal{O}_6^1 = \log(MN)$. *Step 7* considers converting the signal to delay-Doppler domain which is of complexity $\mathcal{O}_7^1 = MN\log(N)$ and *step 10* computes the mean that is considered to have a complexity of $\mathcal{O}_9^1 = 1$ which is calculated L times. Finally, note that *step 6* and *step 7* are computed $\alpha_{\max} \times L$ times, therefore, the computational complexity of Algorithm 1 is found as

$$\mathcal{O}^1 = MN\log(N) + \alpha_{\max}L(\log(MN) + MN\log(N)) + L. \tag{69}$$

2) Fractional Delay Estimation: Algorithm 2 shares all the steps with Algorithm 1. On top of that, in *step 3* the signal is converted to frequency domain with a complexity of $\mathcal{O}_3^2 = MN\log(MN)$. *Step 8* converts back the signal to time domain with a complexity of $\mathcal{O}_8^2 = MN\log(MN)$. Therefore, the total computational complexity of Algorithm 2 is as follows

$$\mathcal{O}^2 = (\alpha_{\max}L + 1)MN\log(MN^2) + \alpha_{\max}L\log(MN) + L. \tag{70}$$

VII. Simulation & Analysis

In this section, we demonstrate the performance of the proposed fractional delay-Doppler channel estimation framework in OTFS system in terms of estimated channel NMSE, bit error rate (BER), and computational complexity. The delay-Doppler grid size is $M = 32$, $N = 32$, the channel model used is Extended Vehicular A model (EVA) [29], and the fractional delay and Doppler shifts are assumed to be uniformly distributed i.e., $(\kappa,\ \iota) \sim \mathcal{U}(-0.5, 0.5)$.

The NMSE of the estimated fractional Doppler shifts κ and fractional delays ι using the proposed algorithms is compared to the NMSE of the optimal estimator that is given by CRLB. The NMSE is calculated as follows

$$\text{NMSE}(\boldsymbol{\eta}) = \frac{1}{L}\sum_{i=1}^{L}\frac{\|\hat{\boldsymbol{\eta}}_i - \boldsymbol{\eta}\|_2^2}{\|\boldsymbol{\eta}\|_2^2}, \tag{71}$$

where $\hat{\boldsymbol{\eta}}_i$ is denotes estimated variable of $\boldsymbol{\eta}$ in the i-th path.

Fig. 4 represents the NMSE vs α for various SNR levels. Fig. 4(a) shows the effect of changing α in the fractional Doppler case while Fig. 4(b) represents the fractional delay case. The

$$\frac{\partial U_z^{(\mathbf{i},\mathbf{f})}}{\partial \kappa_i} = \sum_{q'=0}^{N-1} h_i\Gamma^{(i)}(l,k)\left[\frac{j2\pi(l-l_i)}{MN}\frac{e^{-j2\pi(-q'-\kappa_i)}-1}{Ne^{-j\frac{2\pi}{N}(-q'-\kappa_i)}-N}\right.$$
$$\left. + 2j\pi\frac{e^{-j2\pi(-q'-\kappa_i)}\left(Ne^{-j\frac{2\pi}{N}(-q'-\kappa_i)}-N\right) - e^{-j\frac{2\pi}{N}(-q'-\kappa_i)}\left(e^{-j2\pi(-q'-\kappa_i)}-1\right)}{\left(Ne^{-j\frac{2\pi}{N}(-q'-\kappa_i)}-N\right)^2}\right]$$
$$\cdot\, X\left([l-l_i]_M, [k-k_i+q']_N\right), \tag{66}$$

$$\frac{\partial U_z^{(\mathbf{f},\mathbf{i})}}{\partial \iota_i} = \sum_{q=0}^{M-1} h_i\Gamma^{(i)}(l,k)\left[\frac{-j2\pi k_i}{MN}\frac{e^{j2\pi(-q-\iota_i)}-1}{Me^{j\frac{2\pi}{M}(-q-\iota_i)}-M}\right.$$
$$\left. - 2j\pi\frac{e^{j2\pi(-q-\iota_i)}\left(Me^{j\frac{2\pi}{M}(-q-\iota_i)}-M\right) - e^{j\frac{2\pi}{M}(-q-\iota_i)}\left(e^{-j\frac{2\pi}{N}(-q-\iota_i)}-1\right)}{\left(Me^{j\frac{2\pi}{M}(-q-\iota_i)}-M\right)^2}\right]$$
$$\cdot\, X\left([l-l_i+q]_M, [k-k_i]_N\right). \tag{67}$$

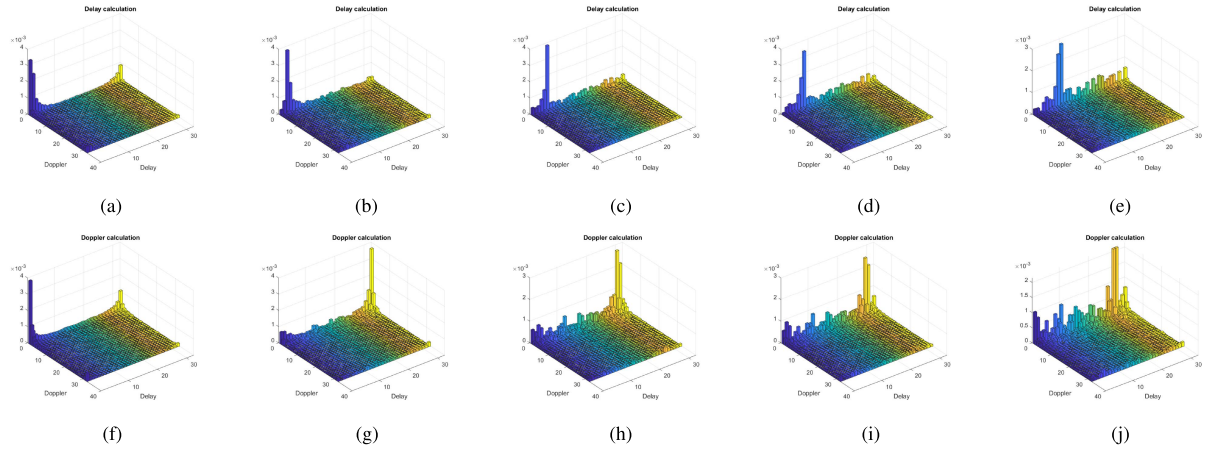

Fig. 8. The delay-Doppler representation of the received pilot signal acquired using experimental setup for different α values. (a) Delay $\alpha = 1$. (b) Delay $\alpha = 10$. (c) Delay $\alpha = 22$. (d) Delay $\alpha = 31$. (e) Delay $\alpha = 40$. (f) Doppler $\alpha = 1$. (g) Doppler $\alpha = 10$. (h) Doppler $\alpha = 22$. (i) Doppler $\alpha = 31$. (j) Doppler $\alpha = 40$.

figures show that as α increases, the normalized error decreases until it reaches a global minimum for an optimal value $\alpha = \alpha_{opt}$. When $\alpha > \alpha_{opt}$, noisy components of the received signal start dominating the higher powers of the signal resulting in an increasing error. Notice that an optimum value of α_{opt} needs to be extracted for each SNR level in both fractional Doppler and delay cases. For instance, for the given simulation parameters, it is found that for $\text{SNR}_p = 40$ dB, the optimal values of alpha are $\alpha_{opt} = 64$ for estimating fractional Doppler shifts as depicted in Fig. 4(a) and $\alpha_{opt} = 79$ for estimating fractional delay shifts as depicted in Fig. 4(b).

Fig. 4 also illustrates the relationship between the NMSE performance and computational complexity for various values of α. Consequently, Fig. 4 assists in determining the appropriate α value based on three criteria: pilot power (SNR_p), RMSE performance, and computational complexity. The chosen α value is denoted by optimum α_{opt} as explained in Section V-E.

Fig. 5(a)–(b) represent the NMSE vs SNR for different α values for fractional Doppler and delay cases, respectively. It is shown that choosing a fixed value of α leads to high-error performance even with a high chosen α value. However, with an optimum α_{opt} value at each SNR level, the system performance almost reaches the lower bound error (i.e., CRLB curve) in both fractional Doppler and delay cases. This means that the proposed estimator is indeed an efficient estimator if $\alpha = \alpha_{opt}$. Furthermore, to emphasize the superiority of the developed estimation framework, the estimation performance of κ is compared to the method in [21] as depicted in Fig. 5(a). It is seen that the proposed method outperforms the sparse structured signal recovery estimator in [21].

The BER analysis is made for OTFS with both fractional delay and Doppler shifts, as illustrated in Fig. 6. BER is simulated vs different SNR_p values and then compared with perfect channel estimation and integer channel ($\kappa = \iota = 0$) cases. It is observed that the BER reduces as SNR_p increases, leading to a system with a performance close to the perfect one that provides more accurate channel estimation and better equalization and data detection. Note that choosing SNR_p is a crucial design parameter; for instance, for the given simulation parameters, $\text{SNR}_p = [20, 25, 30]$ values should not be used since they result in a very poor BER performance.

Fig. 7 illustrates the computational complexity of the proposed method for a fixed number of Doppler bins $N = 32$ and with different number of delay bins M compared to the method in [22]. It is shown that the proposed method has a very low computational complexity compared to the off-grid method in [22] where it could achieve almost 100000 times lower complexity at $M = 32$. Moreover, note that the computational complexity of the proposed method is also adjustable based on the required application by selecting different values of $\alpha_{\max}$.

Finally, we demonstrate the feasibility of our proposed framework for jointly estimating fractional delay and Doppler shifts in a real-time experiment. The experiment was conducted using the Keysight Agilent Technologies EXA vector signal analyzer (VSA) N9010A and EXG vector signal generator (VSG) N5172B, a reverberation chamber, and a fan to generate Doppler. An OTFS frame with parameters $M = 32, N = 32$, a bandwidth of 10 MHz, and a central frequency of 2.45 GHz was transmitted, and the received signal was demodulated and extracted from the VSA, as shown in Fig. 8. The proposed algorithm was then tested by iterating through various values of α given that $\alpha_{\max} = 40$. Fig. 8(a)–(e) depict the case of estimating the delays when $\alpha = [1, 10, 22, 30, 40]$, where it is seen that as α increases, the 2D sinc pulse shifts in the delay axis. The same thing can be seen for the Doppler case, shown by Fig. 8(f)–(j), where this time as α increases, the 2D sinc pulse shifts in the Doppler axis. Using the results in Fig. 8, Algorithms 1 and 2 can be applied to estimate the fractional delay and Doppler shifts, which are computed to be

$$l_i + \iota_i = 0.225, \qquad k_i + \kappa_i = -0.1. \tag{72}$$

These experimental results confirm the effectiveness of our proposed algorithm in estimating fractional channels.

VIII. Conclusion

OTFS has garnered increasing attention over recent years due to its benefits for mobile environments. However, most academic works pertaining to OTFS assume integer delays and Doppler shifts. This is only possible in the case of extremely large bandwidths and frame durations, which is not realistic in practical systems. In most scenarios, the system will suffer from

fractional delay and Doppler shifts, leading to IDI and IDeI. This necessitates a framework for the estimation of fractional delay and Doppler channels. In this paper, we have proposed a framework to estimate OTFS channels with fractional delays and Doppler shifts, allowing flexible OTFS frame design to fulfill various applications and user requirements. A pulsone, which holds its shape under the operations of time delay and Doppler shift as well as being self-dual between time and frequency, is adopted for the estimation by raising the received pilot pulsone to higher powers in both time and frequency domains to estimate fractional Doppler and delay shifts, respectively. In order to assess the estimation performance of the proposed technique, the CRLB has been developed. It has been demonstrated that the proposed framework performs optimally near CRLB.

ACKNOWLEDGMENT

The authors thank TUBITAK for their supports.

REFERENCES

[1] Z. Zhang et al., "6G wireless networks: Vision, requirements, architecture, and key technologies," *IEEE Veh. Technol. Mag.*, vol. 14, no. 3, pp. 28–41, Sep. 2019.
[2] F. Tariq, M. R. Khandaker, K.-K. Wong, M. A. Imran, M. Bennis, and M. Debbah, "A speculative study on 6G," *IEEE Wireless Commun.*, vol. 27, no. 4, pp. 118–125, Aug. 2020.
[3] M. S. J. Solaija, S. E. Zegrar, and H. Arslan, "Orthogonal frequency division multiplexing: The way forward for 6G physical layer design?," *IEEE Veh. Technol. Mag.*, vol. 19, no. 1, pp. 45–54, Mar. 2024.
[4] M. Aldababsa, S. Özyurt, G. K. Kurt, and O. Kucur, "A survey on orthogonal time frequency space modulation," *IEEE Open J. Commun. Soc.*, vol. 5, pp. 4483–4518, 2024, doi: 10.1109/OJCOMS.2024.3422801.
[5] F. Hlawatsch and G. Matz, *Wireless Communications Over Rapidly Time-Varying Channels*. New York, NY, USA: Academic press, 2011.
[6] R. Hadani et al., "Orthogonal time frequency space modulation," in *Proc. IEEE Wireless Commun. Netw. Conf.*, 2017, pp. 1–6.
[7] R. Hadani et al., "Orthogonal time frequency space (OTFS) modulation for millimeter-wave communications systems," in *Proc. IEEE MTT-SInt. Microw. Symp.*, 2017, pp. 681–683.
[8] W. Shen, L. Dai, J. An, P. Fan, and R. W. Heath, "Channel estimation for orthogonal time frequency space (OTFS) massive MIMO," *IEEE Trans. Signal Process.*, vol. 67, no. 16, pp. 4204–4217, Aug. 2019.
[9] Y. Liu, S. Zhang, F. Gao, J. Ma, and X. Wang, "Uplink-aided high mobility downlink channel estimation over massive MIMO-OTFS system," *IEEE J. Sel. Areas Commun.*, vol. 38, no. 9, pp. 1994–2009, Sep. 2020.
[10] W. Yuan, S. Li, Z. Wei, J. Yuan, and D. W. K. Ng, "Data-aided channel estimation for OTFS systems with a superimposed pilot and data transmission scheme," *IEEE Wireless Commun. Lett.*, vol. 10, no. 9, pp. 1954–1958, Sep. 2021.
[11] O. K. Rasheed, G. D. Surabhi, and A. Chockalingam, "Sparse delay-doppler channel estimation in rapidly time-varying channels for multiuser OTFS on the uplink," in *Proc. IEEE 91st Veh. Technol. Conf.*, 2020, pp. 1–5.
[12] M. Zhang, F. Wang, X. Yuan, and L. Chen, "2D structured turbo compressed sensing for channel estimation in OTFS systems," in *Proc. IEEE Int. Conf. Commun. Syst.*, 2018, pp. 45–49.
[13] L. Zhao, W.-J. Gao, and W. Guo, "Sparse Bayesian learning of delay-Doppler channel for OTFS system," *IEEE Commun. Lett.*, vol. 24, no. 12, pp. 2766–2769, Dec. 2020.
[14] P. Raviteja, K. T. Phan, Y. Hong, and E. Viterbo, "Interference cancellation and iterative detection for orthogonal time frequency space modulation," *IEEE Trans. Wireless Commun.*, vol. 17, no. 10, pp. 6501–6515, Oct. 2018.
[15] L. Zhao, W.-J. Gao, and W. Guo, "Embedded delay-Doppler channel estimation for orthogonal time frequency space modulation," in *Proc. IEEE 88th Veh. Technol. Conf.*, 2018, pp. 1–5.
[16] P. Raviteja, K. T. Phan, and Y. Hong, "Embedded pilot-aided channel estimation for OTFS in delay–Doppler channels," *IEEE Trans. Veh. Technol.*, vol. 68, no. 5, pp. 4906–4917, May 2019.
[17] S. S. Das, V. Rangamgari, S. Tiwari, and S. C. Mondal, "Time domain channel estimation and equalization of CP-OTFS under multiple fractional dopplers and residual synchronization errors," *IEEE Access*, vol. 9, pp. 10561–10576, 2021.
[18] D. Shi et al., "Deterministic pilot design and channel estimation for downlink massive MIMO-OTFS systems in presence of the fractional Doppler," *IEEE Trans. Wireless Commun.*, vol. 20, no. 11, pp. 7151–7165, Nov. 2021.
[19] N. Hashimoto, N. Osawa, K. Yamazaki, and S. Ibi, "Channel estimation and equalization for CP-OFDM-based OTFS in fractional doppler channels," in *Proc. IEEE Int. Conf. Commun. Workshops*, 2021, pp. 1–7.
[20] H. B. Mishra, P. Singh, A. K. Prasad, and R. Budhiraja, "OTFS channel estimation and data detection designs with superimposed pilots," *IEEE Trans. Wireless Commun.*, vol. 21, no. 4, pp. 2258–2274, Apr. 2022.
[21] F. Liu, Z. Yuan, Q. Guo, Z. Wang, and P. Sun, "Message passing-based structured sparse signal recovery for estimation of OTFS channels with fractional Doppler shifts," *IEEE Trans. Wireless Commun.*, vol. 20, no. 12, pp. 7773–7785, Dec. 2021.
[22] Z. Wei, W. Yuan, S. Li, J. Yuan, and D. W. K. Ng, "Off-grid channel estimation with sparse Bayesian learning for OTFS systems," *IEEE Trans. Wireless Commun.*, vol. 21, no. 9, pp. 7407–7426, Sep. 2022.
[23] S. E. Zegrar and H. Arslan, "A novel cyclic prefix configuration for enhanced reliability and spectral efficiency in OTFS systems," *IEEE Wireless Commun. Lett.*, vol. 12, no. 5, pp. 888–892, May 2023.
[24] G. D. Surabhi, R. M. Augustine, and A. Chockalingam, "On the diversity of uncoded OTFS modulation in doubly-dispersive channels," *IEEE Trans. Wireless Commun.*, vol. 18, no. 6, pp. 3049–3063, Jun. 2019.
[25] A. V. Oppenheim, *Discrete-Time Signal Processing*. Hoboken, NJ, USA: Pearson Education India, 1999.
[26] Z. Wei, W. Yuan, S. Li, J. Yuan, and D. W. K. Ng, "Performance analysis and window design for channel estimation of OTFS modulation," in *Proc. IEEE Int. Conf. Commun.*, 2021, pp. 1–7.
[27] P. Duhamel, "Implementation of "Split-radix" FFT algorithms for complex, real, and real-symmetric data," *IEEE Trans. Acoust., Speech, Signal Process.*, vol. 34, no. 2, pp. 285–295, Apr. 1986.
[28] S. E. Zegrar and H. Arslan, "Common CP-OFDM transceiver design for low-complexity frequency domain equalization," *IEEE Wireless Commun. Lett.*, vol. 11, no. 7, pp. 1349–1353, Jul. 2022.
[29] 3rd Generation Partnership Project, "Evolved universal terrestrial radio access (E-UTRA); base station (BS) radio transmission and reception," 3rd Generation Partnership Project, Sophia Antipolis, Tech. Specification (TS) 36.104, version 13.2.0, 2016.

Salah Eddine Zegrar (Member, IEEE) received the B.E. degree in electrical and electronics engineering from Gebze Technical University, Gebze, Türkiye, in 2019, and the Ph.D. degree from Istanbul Medipol University, Istanbul, Türkiye, in 2024. Since 2024, he has been a Senior Engineer of the ULAK Haberleşme 6G Research and Development Team, Istanbul. His research interests include 5G and beyond radio access technologies, waveform design, joint radar (sensing) and communication designs, physical layer security, interference management, backscatter communication, and next-generation Wi-Fi.

Ahmet Sacid Sümer received the B.S. degree in electronic and communication engineering from Istanbul Technical University, Istanbul, Türkiye, in 2021. He is currently working toward the Ph.D. degree with the Communications, Signal Processing, and Networking Center, Istanbul Medipol University, Istanbul. His research interests include wireless communications, with an emphasis on multiple access, waveform design, relay transmission, and public safety communication.

Hüseyin Arslan (Fellow, IEEE) received the B.S. degree in electrical and electronics engineering from Middle East Technical University, Ankara, Türkiye, in 1992, and the M.S. and Ph.D. degrees in electrical engineering from Southern Methodist University, Dallas, TX, USA, in 1994 and 1998, respectively. He is a Professor of electrical engineering and the Dean of the School of Engineering and Natural Sciences, Istanbul Medipol University, Istanbul, Türkiye.